

2-2008

# Dynamics In The Transient Complex Of Plastocyanin-cytochrome F From Prochlorothrix Hollandica

Rinske Hulsker

Maria Baranova

George S. Bullerjahn

*Bowling Green State University - Main Campus, bullerj@bgsu.edu*

Marcellus Ubbink

Follow this and additional works at: [http://scholarworks.bgsu.edu/bio\\_sci\\_pub](http://scholarworks.bgsu.edu/bio_sci_pub)



Part of the [Biology Commons](#)

---

## Repository Citation

Hulsker, Rinske; Baranova, Maria; Bullerjahn, George S.; and Ubbink, Marcellus, "Dynamics In The Transient Complex Of Plastocyanin-cytochrome F From Prochlorothrix Hollandica" (2008). *Biological Sciences Faculty Publications*. Paper 42.  
[http://scholarworks.bgsu.edu/bio\\_sci\\_pub/42](http://scholarworks.bgsu.edu/bio_sci_pub/42)

This Article is brought to you for free and open access by the Biological Sciences at ScholarWorks@BGSU. It has been accepted for inclusion in Biological Sciences Faculty Publications by an authorized administrator of ScholarWorks@BGSU.

## Dynamics in the Transient Complex of Plastocyanin–Cytochrome *f* from *Prochlorothrix hollandica*

Rinske Hulsker,<sup>†</sup> Maria V. Baranova,<sup>‡</sup> George S. Bullerjahn,<sup>‡</sup> and Marcellus Ubbink<sup>\*,†</sup>

Leiden Institute of Chemistry, Leiden University, Gorlaeus Laboratories, P.O. Box 9502, 2300 RA Leiden, The Netherlands, Department of Biological Sciences, Bowling Green State University, Bowling Green, Ohio 43403

Received September 27, 2007; E-mail: m.ubbink@chem.leidenuniv.nl

**Abstract:** The nature of transient protein complexes can range from a highly dynamic ensemble of orientations to a single well-defined state. This represents variation in the equilibrium between the encounter and final, functional state. The transient complex between plastocyanin (Pc) and cytochrome *f* (cyt*f*) of the cyanobacterium *Prochlorothrix hollandica* was characterized by NMR spectroscopy. Intermolecular pseudocontact shifts and chemical shift perturbations were used as restraints in docking calculations to determine the structure of the wild-type Pc–cyt*f* complex. The orientation of Pc is similar to orientations found in Pc–cyt*f* complexes from other sources. Electrostatics seems to play a modest role in complex formation. A large variability in the ensemble of lowest energy structures indicates a dynamic nature of the complex. Two unusual hydrophobic patch residues in Pc have been mutated to the residues found in other plastocyanins (Y12G/P14L). The binding constants are similar for the complexes of cyt*f* with wild-type Pc and mutant Pc, but the chemical shift perturbations are smaller for the complex with mutant Pc. Docking calculations for the Y12G/P14L Pc–cyt*f* complex did not produce a converged ensemble of structures. Simulations of the dynamics were performed using the observed averaged NMR parameters as input. The results indicate a surprisingly large amplitude of mobility of Y12G/P14L Pc within the complex. It is concluded that the double mutation shifts the complex further from the well-defined toward the encounter state.

### Introduction

Recent studies have shown the existence of dynamic encounter complexes in transient protein–protein and protein–DNA interactions.<sup>1–3</sup> The encounter state (or encounter complex) is thought to precede the well-defined (or single-orientation) complex as illustrated in a two-step model for protein complex formation (Figure 1). In earlier studies, transient protein complexes were found to range from entirely dynamic to mostly well-defined.<sup>4–12</sup> The complex of plastocyanin (Pc) and cytochrome *f* (cyt*f*) is an interesting example in this respect, because



**Figure 1.** Model for the formation of a protein complex.<sup>2</sup> Free proteins (A) associate to form an encounter complex (B) consisting of an ensemble of protein orientations, which is in equilibrium with a single-orientation complex (C).

comparative studies have shown that the degree of dynamics within the complex varies strongly between species.

The soluble plastocyanin transfers electrons in oxygenic photosynthesis between the membrane-bound cytochrome *b<sub>6</sub>f* and photosystem I complexes.<sup>13,14</sup> Pc is a small (~11 kDa) blue copper protein, which contains a type I copper site for electron transfer.<sup>15,16</sup> Cyt*f* is a *c*-type heme containing cytochrome, of which the truncated N-terminal soluble part (~28 kDa) is used for in vitro experiments (refs 17–19 and references therein). Because of the transient nature of the complex all structures of

<sup>†</sup> Leiden University.

<sup>‡</sup> Bowling Green State University.

- (1) Iwahara, J.; Clore, G. M. *Nature* **2006**, *440*, 1227–1230.
- (2) Volkov, A. N.; Worrall, J. A. R.; Holtzmann, E.; Ubbink, M. *Proc. Natl. Acad. Sci. U.S.A.* **2006**, *103*, 18945–18950.
- (3) Tang, C.; Iwahara, J.; Clore, G. M. *Nature* **2006**, *444*, 383–386.
- (4) Crowley, P. B.; Otting, G.; Schlarb-Ridley, B. G.; Canters, G. W.; Ubbink, M. *J. Am. Chem. Soc.* **2001**, *123*, 10444–10453.
- (5) Garrett, D. S.; Seok, Y. J.; Peterkofsky, A.; Gronenborn, A. M.; Clore, G. M. *Nat. Struct. Biol.* **1999**, *6*, 166–173.
- (6) Liang, Z. X.; Jiang, M.; Ning, Q.; Hoffman, B. M. *J. Biol. Inorg. Chem.* **2002**, *7*, 580–588.
- (7) Liang, Z. X.; Nocek, J. M.; Huang, K.; Hayes, R. T.; Kurnikov, I. V.; Beratan, D. N.; Hoffman, B. M. *J. Am. Chem. Soc.* **2002**, *124*, 6849–6859.
- (8) Ubbink, M.; Ejdebäck, M.; Karlsson, B. G.; Bendall, D. S. *Structure* **1998**, *6*, 323–335.
- (9) Volkov, A. N.; Ferrari, D.; Worrall, J. A. R.; Bonvin, A. M. J. J.; Ubbink, M. *Protein Sci.* **2005**, *14*, 799–811.
- (10) Worrall, J. A. R.; Liu, Y. J.; Crowley, P. B.; Nocek, J. M.; Hoffman, B. M.; Ubbink, M. *Biochemistry* **2002**, *41*, 11721–11730.
- (11) Worrall, J. A. R.; Reinle, W.; Bernhardt, R.; Ubbink, M. *Biochemistry* **2003**, *42*, 7068–7076.

- (12) Hoffman, B. M.; Celis, L. M.; Cull, D. A.; Patel, A. D.; Seifert, J. L.; Wheeler, K. E.; Wang, J. Y.; Yao, J.; Kurnikov, I. V.; Nocek, J. M. *Proc. Natl. Acad. Sci. U.S.A.* **2005**, *102*, 3564–3569.
- (13) Hope, A. B. *Biochim. Biophys. Acta* **2000**, *1456*, 5–26.
- (14) Nelson, N.; Ben Shem, A. *Nat. Rev. Mol. Cell Biol.* **2004**, *5*, 971–982.
- (15) Sykes, A. G. *Struct. Bond.* **1991**, *75*, 175–224.
- (16) Sigfridsson, K. *Photosynth. Res.* **1998**, *57*, 1–28.
- (17) Bendall, D. S. *Photosynth. Res.* **2004**, *80*, 265–276.
- (18) Cramer, W. A.; Soriano, G. M.; Ponomarev, M.; Huang, D.; Zhang, H.; Martinez, S. E.; Smith, J. L. *Annu. Rev. Plant Physiol. Plant Mol. Biol.* **1996**, *47*, 477–508.
- (19) Gray, J. C. *Photosynth. Res.* **1992**, *34*, 359–374.

Pc–cyt*f* complexes determined so far have been determined by NMR spectroscopy.<sup>4,8,20,21</sup> The first structure of the plant complex revealed an electron-transfer pathway between the hydrophobic patch surrounding the copper site of Pc and heme ligand Tyr1 in cyt*f*.<sup>8</sup> Kinetic studies in vitro<sup>13,22–27</sup> have shown that electrostatics play an important role in complex formation. In vivo studies suggest, however, that charged residues are not relevant for fast electron-transfer reactions.<sup>28,29</sup> Nonetheless, the structure of the plant complex showed that the acidic “eastern” patch on Pc interacts with a set of basic residues in the small domain of cyt*f*. The results suggested that this complex is mostly in a well-defined state. The structure of the complex from cyanobacterium *Nostoc* sp. PCC 7119 (former *A. variabilis*) is similar to that from plants, yet the interaction charges between Pc and cyt*f* are interchanged.<sup>21</sup> The complex of *Phormidium laminosum* Pc and cyt*f* demonstrated that the charge interactions are not absolutely necessary for a functional complex. In this case, the proteins mostly interact through hydrophobic contacts. The structure showed poorer convergence to a well-defined state, suggesting more dynamics within the complex.<sup>4</sup>

Plastocyanin from cyanobacterium *Prochlorothrix hollandica* contains two unusual residues located in the hydrophobic patch, which have been mutated to the residues normally found in these positions (Tyr12Gly/Pro14Leu). The mutant Pc has been shown to react differently with photosystem I<sup>30</sup> and was suggested to be more dynamic in complex with cyt*f* from *Ph. laminosum*.<sup>31</sup> Here, we report the structure of the physiological complex between *P. hollandica* Pc and cyt*f* and show that the existing equilibrium between encounter and well-defined state in the complex is shifted toward the encounter state by the mutation of two unusual hydrophobic patch residues (Y12G/P14L). It is concluded that this complex is on the border between dynamic and well-defined states.

## Materials and Methods

**Protein Expression and Purification.** Mutant and wild-type <sup>15</sup>N-labeled *P. hollandica* plastocyanin were expressed and purified as described before.<sup>31</sup> Cyt*f* was expressed and purified essentially as described,<sup>32</sup> in which the coding sequence of the *P. hollandica* cyt*f* soluble domain (GenBank AF486288) was ligated in-frame to the *Ph. laminosum* Pc leader coding sequence and expressed in *Escherichia coli*. The purification procedure followed the protocol for the *Ph. laminosum* protein.<sup>32</sup> Yields of pure cyt*f* were typically 3 mg protein per liter of culture.

**Cd-Substitution of Pc.** Cd-substitution of plastocyanin was essentially done as described<sup>33</sup> with the following modifications. Of a 200 mM KCN, 500 mM Tris/HCl, pH 7.0 solution, 0.5 mL was added to 0.5 mL of 1 mM oxidized Pc. The sample was then loaded on a G25 Sephadex column pre-equilibrated with 1 mM CdCl<sub>2</sub>, 50 mM HEPES, pH 7.0. The buffer was exchanged to water and then to 10 mM sodium phosphate, pH 6.0.

**NMR Samples.** All protein samples contained 10 mM sodium phosphate, pH 6.0, 6% D<sub>2</sub>O. Protein concentrations were determined by optical spectroscopy using  $\epsilon_{602}$  of 4.9 mM<sup>−1</sup> cm<sup>−1</sup> for oxidized Cu–plastocyanin (PCu),  $\epsilon_{554}$  of 24.9 mM<sup>−1</sup> cm<sup>−1</sup> for reduced cyt*f*, and  $\epsilon_{278}$  of 7.6 mM<sup>−1</sup> cm<sup>−1</sup> for Cd–plastocyanin (PCd) ( $\epsilon_{278}$  based on atomic absorption measurements). The pH was adjusted with microliter aliquots of 0.1 or 0.5 M HCl. Samples for assignment contained 1.0 mM <sup>15</sup>N-labeled PCd. For titrations, both Cu(II) and Cd-substituted <sup>15</sup>N-labeled Pc were concentrated to 0.2 mM. Wild-type PCd could not be used for titrations because of unfolding in the presence of high amounts of cyt*f*. This was not the case for the mutant PCd, which is more stable in both the Cu- and Cd-substituted form. The copper proteins were reduced by addition of 2.0 mM ascorbate and flushed with argon to prevent reoxidation. Aliquots of a 1.33 mM cyt*f* stock solution were added to the Pc containing samples. Samples for determination of PCS contained 85  $\mu$ M <sup>15</sup>N-labeled wild type or mutant PCd and 50 or 100  $\mu$ M oxidized cyt*f*, respectively. Cyt*f* was subsequently reduced in the sample by addition of 20 equiv of sodium ascorbate. The pH was measured before and after each experiment.

**NMR Spectroscopy.** All NMR spectra were recorded at 300 K on a Bruker DMX600 spectrometer equipped with a triple-resonance TCI-ZGRAD ATM Cryoprobe (Bruker, Karlsruhe, Germany). Chemical-shift perturbation and pseudocontact shift(s) (PCS) studies were performed by acquiring <sup>15</sup>N,<sup>1</sup>H HSQC (heteronuclear single quantum coherence spectra). Spectral widths of 40 ppm (<sup>15</sup>N) and 13.5 ppm (<sup>1</sup>H) were used, and 1024 and 256 complex points were acquired in the direct and indirect dimension, respectively. Cd-substituted wild-type and mutant Pc resonances were assigned using 3D NOESY-HSQC and 3D TOCSY-HSQC experiments. Data were processed with AZARA 2.7<sup>34</sup> and analyzed in ANSIG for Windows.<sup>35</sup>

**Binding Curves and Chemical Shift Mapping.** Averaged chemical shift perturbations ( $\Delta\delta_{\text{avg}}$ ) were derived from the following equation:

$$\Delta\delta_{\text{avg}} = \sqrt{\frac{1}{2} \left( \frac{\Delta\delta_{\text{N}}^2}{25} + \Delta\delta_{\text{H}}^2 \right)} \quad (1)$$

where  $\Delta\delta_{\text{N}}$  and  $\Delta\delta_{\text{H}}$  are the chemical shift perturbation after extrapolation to the 100% bound state of the amide nitrogen and proton, respectively.<sup>36</sup> Chemical shift titration curves were analyzed with a two-parameter nonlinear least-squares global fit to a 1:1 binding model, which corrects for dilution effects:<sup>11,23</sup>

$$\Delta\delta_{\text{bind}} = \frac{1}{2} \Delta\delta_{\text{max}} (A - \sqrt{A^2 - 4R}) \quad (2a)$$

$$A = 1 + R + \frac{PR + C}{PCK_a} \quad (2b)$$

where  $R$  is the [cyt*f*]:[<sup>15</sup>N-Pc] ratio,  $\Delta\delta_{\text{bind}}$  is the chemical shift perturbation at a given  $R$ ,  $\Delta\delta_{\text{max}}$  is the chemical shift perturbation at 100% bound <sup>15</sup>N-Pc,  $P$  is the initial [<sup>15</sup>N-Pc],  $C$  is the stock concentration of cyt*f* and  $K_a$  is the association constant of the complex.

- (20) Lange, C.; Cornvik, T.; Díaz-Moreno, I.; Ubbink, M. *Biochim. Biophys. Acta* **2005**, *1707*, 179–188.
- (21) Díaz-Moreno, I.; Díaz-Quintana, A.; De la Rosa, M. A.; Ubbink, M. *J. Biol. Chem.* **2005**, *280*, 18908–18915.
- (22) Beoku-Betts, D.; Chapman, S. K.; Knox, C. V.; Sykes, A. G. *Inorg. Chem.* **1985**, *24*, 1677–1681.
- (23) Kannt, A.; Young, S.; Bendall, D. S. *Biochim. Biophys. Acta* **1996**, *1277*, 115–126.
- (24) Niwa, S.; Ishikawa, H.; Nikai, S.; Takabe, T. *J. Biochem.* **1980**, *88*, 1177–1183.
- (25) Qin, L.; Kostić, N. M. *Biochemistry* **1992**, *31*, 5145–5150.
- (26) Takabe, T.; Ishikawa, H. *J. Biochem.* **1989**, *105*, 98–102.
- (27) Takenaka, K.; Takabe, T. *J. Biochem.* **1984**, *96*, 1813–1821.
- (28) Soriano, G. M.; Ponamarev, M. V.; Tae, G. S.; Cramer, W. A. *Biochemistry* **1996**, *35*, 14590–14598.
- (29) Zhou, J. H.; Fernández-Velasco, J. G.; Malkin, R. J. *Biol. Chem.* **1996**, *271*, 6225–6232.
- (30) Navarro, J. A.; Myshkin, E.; De la Rosa, M. A.; Bullerjahn, G. S.; Hervás, M. *J. Biol. Chem.* **2001**, *276*, 37501–37505.
- (31) Crowley, P. B.; Vintonenon, N.; Bullerjahn, G. S.; Ubbink, M. *Biochemistry* **2002**, *41*, 15698–15705.
- (32) Schlär, B. G.; Wagner, M. J.; Vijgenboom, E.; Ubbink, M.; Bendall, D. S.; Howe, C. J. *Gene* **1999**, *234*, 275–283.

- (33) Ubbink, M.; Lian, L. Y.; Modi, S.; Evans, P. A.; Bendall, D. S. *Eur. J. Biochem.* **1996**, *242*, 132–147.
- (34) Boucher, W. AZARA 2.7; Department of Biochemistry, University of Cambridge: Cambridge, U.K., 2002.
- (35) Helgstrand, M.; Kraulis, P.; Allard, P.; Härd, T. *J. Biomol. NMR* **2000**, *18*, 329–336.
- (36) Grzesiek, S.; Bax, A.; Clore, G. M.; Gronenborn, A. M.; Hu, J. S.; Kaufman, J.; Palmer, I.; Stahl, S. J.; Wingfield, P. T. *Nat. Struct. Biol.* **1996**, *3*, 340–345.

**Table 1.** Restraint Groups

type	number	scale	number × scale
interface	22	10	220
pseudocontact	36	10	360
minimal distance	94	3	282
angle	36	<i>a</i>	<i>a</i>

<sup>a</sup> Scaling of the angle restraints is not comparable to the other (distance) restraints.

**Structure Determination.** The coordinates for *P. hollandica* Pc were taken from the solution structure (PDB entry 1B3I<sup>37</sup>). Mutations Y12G and P14L were introduced in silico, using DeepView/Swiss-PdbViewer version 3.7.<sup>38</sup> A model of *P. hollandica* cytf based on *Ph. laminosum* cytf (PDB entry 1CI3<sup>39</sup>) was created with MODELLER 6v2.<sup>40</sup> Docking of Pc onto cytf was done using restrained rigid body molecular dynamics in XPLOR-NIH 2.9.9.<sup>41</sup> The coordinates of cytf were fixed, while Pc was placed at a random position and allowed to move under the forces of restraints and a van der Waals repel function. Only the interactions between the backbone and C $\beta$  atoms of Pc and all atoms of cytf were considered at this stage. The restraints were divided into three classes. Chemical shift perturbations in the presence of reduced cytf were attributed to the proximity of the protein. The average relative solvent-accessible surface area of each Pc residue was calculated with NACCESS 2.1.1.<sup>42</sup> Residues with a surface accessible surface area of more than 50% and  $\Delta\delta_{\text{bind}} \geq 0.1$  (<sup>15</sup>N) or 0.02 (<sup>1</sup>H) were included in the class for interface restraints. Pseudocontact and angle restraints based on PCS were defined as described.<sup>8</sup> Residues that do not experience a PCS were included in a minimal distance restraint class. A summary of the restraints is given in Table 1. The product of the number of restraints and the scale used in the calculations indicates the weight of each group. The rigid-body molecular dynamics was essentially done as described before.<sup>4,8,20,21</sup> A run comprised 3000 cycles, each of 1000 steps. Structures below an energy threshold were saved, yielding ~200 structures per run. To obtain multiple independent dockings during a run Pc was randomly displaced after having reached an energy minimum, with energies changing less than 2-fold during 10 cycles. Approximately 130 displacements occurred per run. The resulting structures were ranked according to total restraint energy, and the lowest energy structures were subjected to energy minimization of the side chains in the interface. This ensemble of 20 lowest energy structures has been deposited in the Protein Data Bank (entry 2P80). Figures 3, 5, and 8 were made in PyMOL v0.98.<sup>43</sup> The buried interface area was calculated using NACCESS.

**Pseudocontact Simulations.** The PCS simulations were done using XPLOR-NIH. The lowest energy structure of wild-type Pc–cytf was used as the initial orientation of the Y12G/P14L Pc–cytf complex. The relative diffusional movement in the mutant complex of Pc–cytf was decomposed into two types of rotations. Pc was rotated around its center of mass (wobble) and around the origin of the magnetic susceptibility tensor frame; the heme iron in cytf (rotation). For this purpose three pseudoatoms, representing the magnetic susceptibility tensor were placed at 2 Å from the heme metal center in cytf. They were used as a reference frame with the  $\chi_{zz}$  component of the tensor placed along the Fe–Tyr1N vector. Each rotation was again decomposed in three directions (X, Y, and Z), resulting in sets of six variables for the complete movement. For a given set (for example, 40°, 80°, 35°/60°, 60°, 60°)

an ensemble of 50 structures was created by six rotations over random angles within the range given for each of the six variables (i.e., between 0° and 40° for the first angle, and so on), and this procedure was repeated 50 times. For such an ensemble the average PCS was calculated for each Pc nucleus. The equation used to calculate PCS, assuming an axial magnetic susceptibility tensor, oriented along the Fe–Tyr1N vector<sup>8</sup> is

$$\Delta\delta_{\text{PC}} = \frac{10^{36}F}{12\pi N_A r^3} \chi_{\text{ax}} (3 \cos^2 \theta - 1) \quad (3)$$

where  $\Delta\delta_{\text{PC}}$  is the size of the PCS in ppm,  $r$  is the distance (Å) from the Pc nucleus to the iron, and  $\theta$  is the angle between the nucleus, the iron, and the nitrogen of the N-terminal amino group of cytf.  $F$  reflects the fraction Pc in complex with cytf; the value used in these simulations is 0.7.  $N_A$  is Avogadro's number and  $\chi_{\text{ax}}$  the size of the magnetic susceptibility tensor, taken to be  $2.0 \times 10^{-8} \text{ m}^3 \text{ mol}^{-1}$ , on the basis of other *c*-type cytochromes.<sup>44</sup>

If the rotations caused the structures to either clash or not touch, the distance was increased or decreased in steps of 1 Å, respectively, until both proteins were just in contact. To determine the correlation between the observed and simulated PCS the  $Q$ -factor was calculated with the following equation:

$$Q = \left[ \sum_i \{ \Delta\delta_{\text{PC}}^{\text{obs}}(i) - \Delta\delta_{\text{PC}}^{\text{sim}}(i) \}^2 / \sum_i \Delta\delta_{\text{PC}}^{\text{obs}}(i)^2 \right]^{1/2} \quad (4)$$

where  $\Delta\delta_{\text{PC}}^{\text{obs}}$  is the size of the observed PCS in ppm and  $\Delta\delta_{\text{PC}}^{\text{sim}}$  is the size of the average simulated PCS for residue  $i$ .

## Results and Discussion

**Complex of *P. hollandica* PCu and cytf: Wild-Type versus Y12G/P14L Pc.** To compare the effects of binding, chemical shift perturbations were analyzed for wild-type and Y12G/P14L *P. hollandica* Pc upon titration with cytf. The presence of reduced cytf gives rise to distinct changes in the <sup>1</sup>H–<sup>15</sup>N HSQC spectrum of <sup>15</sup>N–PCu(I). A single averaged resonance was observed for each amide indicating that exchange between free and bound Pc is fast on the NMR-time scale. The observed chemical shift changes ( $\Delta\delta_{\text{bind}}$ ) of the most affected residues were plotted against the molar ratio of cytf: <sup>15</sup>N–PCu (Figure 2) and fitted to a 1:1 binding model.<sup>23</sup> This yields a  $K_a$  of  $25 (\pm 2) \times 10^3 \text{ M}^{-1}$  for wild-type PCu and  $20 (\pm 1) \times 10^3 \text{ M}^{-1}$  for Y12G/P14L PCu. Although the binding constants are very similar, there is a significant difference in the size of the chemical shift perturbations. This becomes apparent when the average chemical shift perturbations ( $\Delta\delta_{\text{avg}}$ ) per residue are considered (Figure 3). From the figure, it is clear that the hydrophobic patch surrounding the copper site is the main site involved in complex formation, as seen in Pc–cytf complexes from other organisms.<sup>4,8,20,21,45</sup> The residues that are affected in the wild-type complex are generally also affected in the mutant complex, but the size of the chemical shift changes is clearly smaller, by about 40%. This is comparable to the results obtained for the complex of *P. hollandica* Pc and cytf from *Ph. laminosum*,<sup>31</sup> and suggests increased dynamics in the complex of Y12G/P14L Pc and cytf. A comparison of the size of the PCS found for the complex with wild type and mutant Pc (see later, Figure 7A) supports this notion.

(37) Babu, C. R.; Volkman, B. F.; Bullerjahn, G. S. *Biochemistry* **1999**, *38*, 4988–4995.

(38) Guex, N.; Peitsch, M. C. *Electrophoresis* **1997**, *18*, 2714–2723.

(39) Carrell, C. J.; Schlarb, B. G.; Bendall, D. S.; Howe, C. J.; Cramer, W. A.; Smith, J. L. *Biochemistry* **1999**, *38*, 9590–9599.

(40) Sali, A.; Blundell, T. L. *J. Mol. Biol.* **1993**, *234*, 779–815.

(41) Schwieters, C. D.; Kuszewski, J. J.; Tjandra, N.; Clore, G. M. *J. Magn. Reson.* **2003**, *160*, 65–73.

(42) Hubbard, S. J. and Thornton, J. M. *NACCESS*; Department of Biochemistry and Molecular Biology, University College London: London, 1993.

(43) DeLano, W. L. *The PyMOL Molecular Graphics System 2002*; DeLano Scientific LLC: Palo Alto, CA, 2002.

(44) Worrall, J. A. R.; Kolczak, U.; Canters, G. W.; Ubbink, M. *Biochemistry* **2001**, *40*, 7069–7076.

(45) Crowley, P. B.; Ubbink, M. *Acc. Chem. Res.* **2003**, *36*, 723–730.



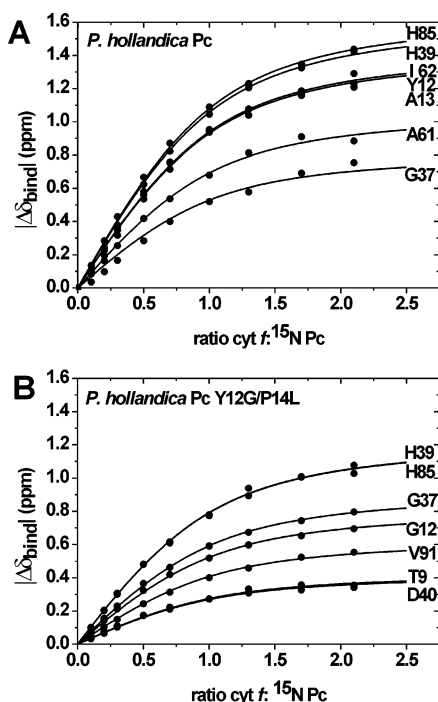


**Figure 2.** Binding curves for complex formation between *P. hollandica* Pc and cytf. The  $|\Delta\delta_{\text{bind}}|$  of individual residues is plotted as a function of the cytf:Pc ratio. Global nonlinear least-squares fits (solid lines) to a 1:1 binding model<sup>23</sup> yielded a  $K_a$  of  $25 (\pm 2) \times 10^3 \text{ M}^{-1}$  for wild-type PCu (A) and  $20 (\pm 1) \times 10^3 \text{ M}^{-1}$  for Y12G/P14L Pc (B).

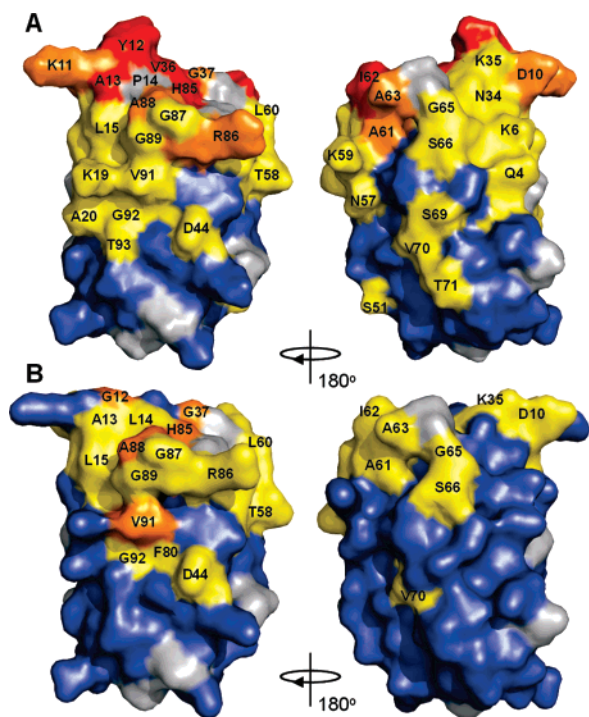


**Figure 3.** Surface representations of (A) *P. hollandica* Pc (PDB file 1BI3) and (B) a model of *P. hollandica* Pc Y12G/P14L. Average chemical shift perturbations ( $\Delta\delta_{\text{avg}}$ ) for PCu are color coded as follows: blue,  $\Delta\delta_{\text{avg}} \leq 0.025 \text{ ppm}$ ; yellow,  $0.025 < \Delta\delta_{\text{avg}} \leq 0.10 \text{ ppm}$ ; orange,  $0.10 < \Delta\delta_{\text{avg}} \leq 0.175 \text{ ppm}$ ; and red,  $\Delta\delta_{\text{avg}} \geq 0.175 \text{ ppm}$ .

The affinity between Pc and cytf decreases with increasing ionic strength (Figure 4). A reduction of  $\Delta\delta_{\text{bind}}$  of 46% at 200 mM NaCl is observed, indicating electrostatics play a role in complex formation. The Pc Y12G/P14L complex is similarly affected by ionic strength, with  $\Delta\delta_{\text{bind}}$  reduced by 42%. This

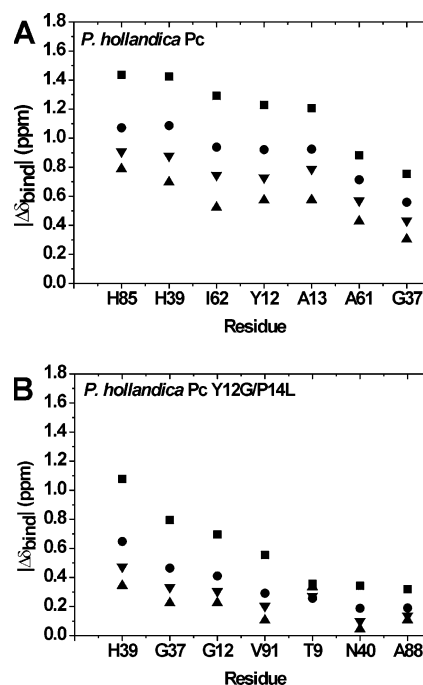


**Figure 4.** Salt dependence of the  $|\Delta\delta_{\text{bind}}|$  of the most shifted residues of wild-type PCu (A) and Y12G/P14L PCu (B) in complex with cytf (the ratio cytf:PCu is 3:1). Symbols indicate the presence of 0 mM NaCl (■), 50 mM NaCl (●), 100 mM NaCl (▼), and 200 mM NaCl (▲).

demonstrates that the effect of ionic strength on complex formation is similar in the wild-type and mutant complexes.

**Structure of the Complex of *P. hollandica* Pc–cytf.** The structure of *P. hollandica* Pc–cytf complex has been determined by rigid-body structure calculations using restraints obtained by NMR spectroscopy. Two types of NMR data were used. One is chemical shift perturbations of solvent exposed Pc residues, which give information on the proximity of these residues to cytf. The other is intermolecular pseudocontact shifts, which are observed in the presence of paramagnetic, oxidized cytf and give both distance and angular information on the proximity of Pc residues to the Fe(III).<sup>8</sup> To be able to study the interaction of Pc with both oxidized and reduced cytf without interference from electron-transfer reactions, the Cu in Pc was substituted with Cd (PCd).

A titration followed by  $^1\text{H}$ - $^{15}\text{N}$  HSQC spectra showed that the complex of PCd Y12G/P14L has a  $K_a$  of  $26 (\pm 3) \times 10^3 \text{ M}^{-1}$ , similar to that of the complex with PCu Y12G/P14L. The observed  $\Delta\delta_{\text{avg}}$  in the mutant PCd complex are identical for forty percent of the perturbed residues, while for residues in the vicinity of the metal site and the “eastern patch”  $\Delta\delta_{\text{avg}}$  values differ between Pc containing Cu(I) and Cd(II). Similar differences have been observed before for *Ph. laminosum* Cd-substituted Pc in complex with cytf<sup>46</sup> and are most likely caused by the charge difference between the metals. Comparison of  $\Delta\delta_{\text{avg}}$  or  $K_a$  between the wild type PCu and PCd complexes was not possible because of experimental limitations (see Materials and Methods).

The rigid body calculations with the restraints summarized in Table 1 converge to an ensemble of complexes, which is depicted by an overlay of the twenty lowest energy structures in Figure 5A. The ensemble is characterized by a Cu–Fe

(46) Crowley, P. B. Transient protein interactions of photosynthetic redox partners. Ph. D. Thesis. Leiden University, Leiden, the Netherlands, 2002.

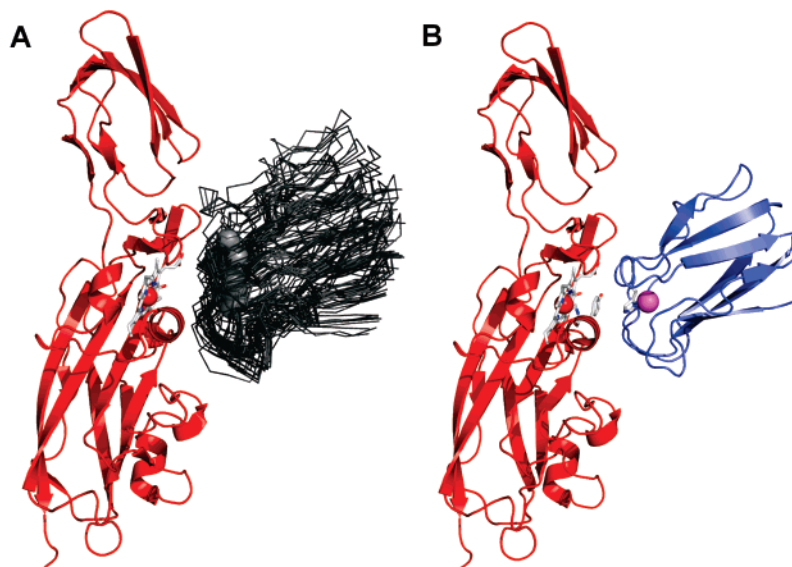


**Figure 5.** Structure of *P. hollandica* Pc–cytf complex: (A) Superposition of the 20 lowest energy conformers. Cytf is shown as a red ribbon, the heme as sticks, and the Fe ion as a sphere; the backbone of Pc is shown as a black C $\alpha$  trace, with the copper ion as a gray sphere. (B) Lowest energy representation, Pc is shown as a blue ribbon, with the Cu ion in magenta. Copper ligand His85 and heme ligand Tyr1 are shown as sticks.

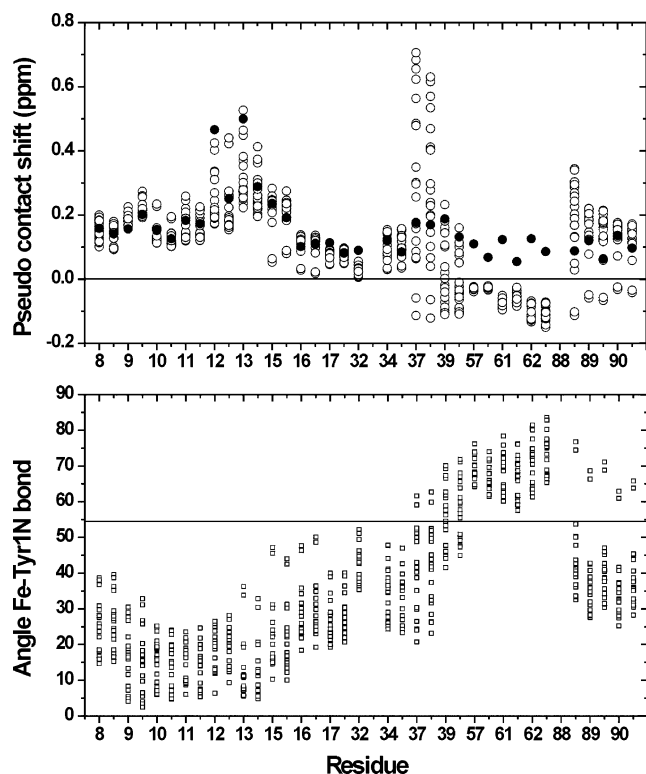


**Figure 6.** Violation analysis for the wild-type Pc–cytf complex. The top panel shows the observed PCS (●) and the back-calculated PCS (○) for the backbone amide atoms in the 20 lowest energy structures. For every residue the  $^{15}\text{N}$  value is shown (major tick), followed by the  $^1\text{H}$  value (minor tick). The bottom panel shows the back-calculated angles (□) between the nucleus, the heme iron, and the Tyr1 N atom. Positive PCS are expected to give an angle  $<54.7^\circ$  (solid line).

distance of  $13.4 \pm 1.4 \text{ \AA}$ . The average positional rmsd from the mean structure of the Pc backbone atoms in the 20 lowest energy structures is  $4.6 \pm 2.7 \text{ \AA}$ . This variability is mainly due to a relative translational displacement of the Pc on the cytf surface. Violation analysis of both angles and PCS (Figure 6) shows that there is a large degree of variation between the structures. In structure calculations of other Pc–cytf complexes

better convergence was observed using similar input.<sup>8,20,21</sup> Therefore, we believe the limited convergence is an indication of real dynamics rather than a lack of sufficient restraints. The observed restraints in this case represent an average that can be approximated by an ensemble of structures. For residues in the loop regions 35–41 and 46–51 of Pc, negative PCS are predicted in part of the structures. This is related to the angle between the nucleus-iron vector and the Fe–Tyr1 N bond, which exceeds  $54.7^\circ$ , resulting in a sign change of the PCS.<sup>47</sup> Both the rmsd and violations for the ensemble indicate that the *P. hollandica* Pc–cytf complex is much more dynamic than the plant and *Nostoc* sp. PCC 7119 complexes<sup>8,21</sup> and more closely resembles the highly dynamic *P. laminosum* complex.<sup>4</sup>

The orientation of wild-type Pc in the lowest energy *P. hollandica* Pc–cytf complex (Figure 5B) is reminiscent of the orientation found for *Nostoc* sp. PCC 7119.<sup>21</sup> The binding interface comprises 15 Pc residues, all located in the hydrophobic patch, including Tyr12 and Pro14. The buried interface area for Pc is calculated to be  $\sim 860 \text{ \AA}^2$ . Similarly, 15 cytf residues and the propionate side chains of the heme contribute to a buried interface area of  $\sim 725 \text{ \AA}^2$ . Although the chemical shift changes in the complex are salt dependent (see earlier) the only charged residues in the interface are Asp63 in cytf, which interacts with Thr58 in Pc and Arg86 in Pc, which could interact with Tyr162 in cytf. Some polar residues are present in the interface, mainly on the cytf side, but clear electrostatic contributions as seen in the plant and *Nostoc* Pc–cytf complexes are not found. The lack of interaction between the eastern patch on Pc and the small domain of cytf as found in the plant and *Nostoc* sp. PCC 7119 complex could account for the more dynamic nature of the *P. hollandica* complex. Such interactions are lacking in the *Ph. laminosum* Pc–cytf complex, which is also very dynamic. In the lowest energy structure the coupling pathway for electron transfer comprises the heme ligand Tyr1 and the solvent-exposed copper ligand His85. This pathway has also been found in plant Pc–cytf complexes.<sup>8,20</sup> It has to be

(47) Arnesano, F.; Banci, L.; Piccioli, M. *Q. Rev. Biophys.* **2005**, *38*, 167–219.

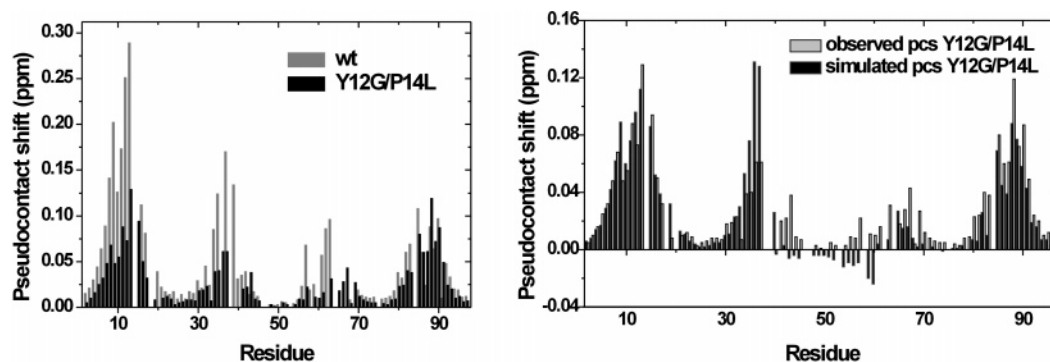


**Figure 7.** (A)  $^1\text{H}$  PCS in wild type and mutant Pc in complex with cyt*f*; (B) observed and simulated  $^1\text{H}$  PCS in mutant Pc in complex with cyt*f*.

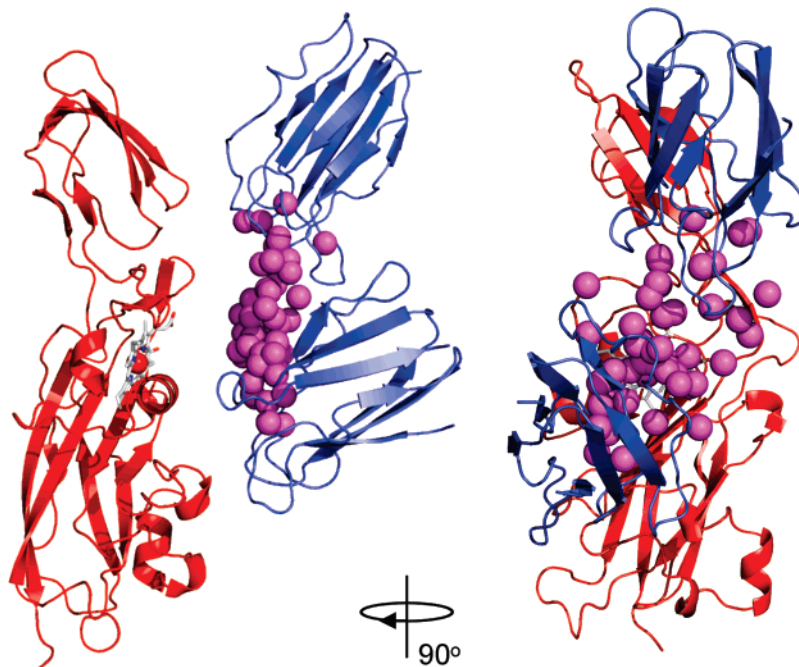


**Figure 8.** Representation of the dynamics in the Pc Y12G/P14L–cyt*f* complex. Cyt*f* is shown as a red ribbon, the heme as sticks, and the Fe ion as a sphere. The Cu ion in a set of 50 Pc Y12G/P14L molecules is shown as magenta spheres. The two most extreme orientations of Pc Y12G/P14L are shown as blue ribbons.

noted that because of the variation in the ensemble a detailed analysis of electron-transfer pathways is not possible.

**Dynamics in *P. hollandica* Y12G/P14L Pc–cyt*f* Complex.** When the PCS in the wild type and Y12G/P14L Pc–cyt*f* complexes are compared a clear decrease in their size for the mutant complex can be observed (Figure 7A), except for the last 10 residues. The decrease in size of chemical shift perturbations (see earlier) and PCS in the mutant complex leads to less and weaker restraints, which in turn cause more possible orientations with similar energies. As a result, rigid-body structure calculations for the *P. hollandica* Y12G/P14L Pc–cyt*f* complex did not lead to any converged ensemble of structures, contrary to the case of the wild-type complex. The inhomogeneous decrease in PCS and lack of convergence of the calculations can be attributed to a more dynamic nature of the Y12G/P14L Pc–cyt*f* complex.

Simulations were done to determine the degree of movement in the mutant complex sufficient to result in the observed averaged PCS (Figure 7A). The orientation of the lowest energy complex between wild-type Pc and cyt*f* was used as a starting point. Rotation of Pc around the Fe axis in each direction was analyzed, an example for 60° is shown in Figure S1. It was

concluded that rotation in a single direction does not result in an ensemble of orientations that closely matches the observed and simulated PCS. The effect of rotation around the center of mass of Pc Y12G/P14L (wobble) of various degrees was analyzed as well (Figure S2). This movement clearly affects the overall size of the average PCS. It has to be noted though, that the chemical shift perturbation map indicates that the binding site is localized mostly at the hydrophobic patch. Thus, an ensemble of orientations that results from this movement over for example 180° is unrealistic. By trying systematically combinations of rotation and wobbling, it was found that rotation of Pc around the Fe with amplitudes of 40°, 80°, and 35° in the *x*-, *y*-, and *z*-direction, respectively, combined with rotation around the center of mass of Pc Y12G/P14L (wobble) of 60° in all directions results in an ensemble of orientations with average PCS values that closely resemble those observed (Figure 7B). This solution is not unique; there are more combinations of variables that lead to similar results. For example rotation of 60°, 90°, and 45° in the *x*-, *y*- and *z*-direction, respectively, combined with rotation around the center of mass of Pc Y12G/P14L (wobble) of 60° in all directions was found to result in very similar average PCS and a similar spread in Pc positions

(Figure S3). Some Pc Y12G/P14L residues have deviating PCS values in all simulations. These residues (33–37 and 57–59) are found in the interface and are also the most violated in the wild-type structure (Figure 6), which suggests that these deviations are not specific for the Y12G/P14L Pc–cyt*f* complex. It must be noted, however, that residues 33–37 are found to be the most affected by the mutations Y12G/P14L apart from residues neighboring the mutations,<sup>31</sup> perhaps indicating a structural difference in this part of the mutant Pc, as compared to the wild type.

The 50 orientations of Pc Y12G/P14L that result from the simulation mentioned above are visualized in Figure 8. From these simulations, it is clear that a considerable range of orientations is sampled in the mutant complex. It also demonstrates that merely the observation of PCS cannot be used as evidence for a well-defined complex. The Cu–Fe distances are mostly too large for electron transfer, so only a subset of states will be suitable for electron transfer. Since the wild-type and mutant complex have similar binding constants and the electron-transfer rates to Pc are similar ( $k_2 = 2\text{--}3 \times 10^8 \text{ M}^{-1} \text{ s}^{-1}$ ; Baranova and Bullerjahn, manuscript in preparation), it provides an example of two complexes that differ mainly in their dynamics.

It can be concluded that the mutation of the two hydrophobic patch residues Tyr12 and Pro14 to the residues found in other plastocyanins, results in a more dynamic complex of Pc and cyt*f*. These mutations provide a way to compare the reasonably well-defined wild-type Pc–cyt*f* complex with one that is more dynamic, presenting an opportunity to examine the movements and dynamics in the encounter state of a transient protein–protein complex.

**Acknowledgment.** C. Erkelens and F. Lefeber are gratefully acknowledged for assistance with the NMR experiments. R.H. and M.U. acknowledge financial support from The Netherlands Organisation for Scientific Research, VIDI-Grant 700.52.425. G.S.B. was supported under award 0070334 from the National Science Foundation.

**Supporting Information Available:** Three figures showing results of PCS simulations for various sets of rotation angles. This material is available free of charge via the Internet at <http://pubs.acs.org>.

JA077453P